Data Compression for Time-Stretch Imaging Based on Differential Detection and Run-Length Encoding

Bo Dai, Songchao Yin, Zhensen Gao, Kaimin Wang, Dawei Zhang, Songlin Zhuang, and Xu Wang, *Senior Member, IEEE*

***Abstract*—A high-fidelity data compression method based on differential detection and run-length encoding is proposed for a time-stretch imaging system, where a spatial image is mapped to the time domain and then read out by a balanced photodetector for image reconstruction. Differential detection is capable of distinguishing discrepancy of consecutive scans and eliminating identical signals. After the detection, run-length encoding merges consecutive identical data to a single data. In the experiment, a 77.76-MHz line-scan imaging system is demonstrated. The compression ratio of more than 3.8 is achieved. After the data decompression, the image of high fidelity can be reconstructed.**

***Index Terms*—Imaging system, optical signal processing, ultrafast measurements.**

I. Introduction

AIMING at observing dynamics and tracking moving objects for discovering the ultrafast process, ultrafast optical imaging is emerging as an important technology in the scientific and industrial fields, including photochemistry, microfluidics, plasma physics, high power laser-material interaction, laser surgery, and intelligent manufacturing [1]–[3]. To achieve ultrafast imaging, a lot of methods have been developed over the past decades, such as in-situ-storage image sensor, framing and streak camera [4], [5]. The widely used streak camera is able to perform single shot imaging and provide the framing rate in the order of tera-frame per second (Tfps). However, strict synchronization between the camera and the event is required. Pump-probe time resolved imaging is another powerful tool to capture ultrafast motion image but it is only suitable for measuring repetitive events, which impedes its applications in capturing natural non-repetitive events [6].

In recent years, a brand new time-stretch imaging technique has been proposed and demonstrated for ultrafast optical imaging [7]. In the time stretch imaging, both spatial and temporal dispersion are exploited to encode the spatial profile of the target into the spectrum of short optical pulse and then map the spectrum into the time domain before photodetection and image reconstruction. The time-stretch imaging technique is capable of realizing phase imaging and capturing the fast dynamics of rare events without the need of repetitive measurement [8], [9]. Since the image information is carried by a serial time-domain data stream, only low-cost single-pixel photodiode is required for image readout. Various schemes have been proposed to improve the time-stretch imaging system. A multi-wavelength time-stretch imaging system was proposed to release the limitation of utilizing an expensive ultra-short pulse source [10]. To eliminate the use of bulky and lossy free-space diffraction gratings, a highly efficient spectrally encoded imaging system has been demonstrated by using a 45° tilted fiber grating [11]. Besides, multiplexing techniques were widely used to improve the system performance. Time-stretch imaging systems employing optical time-division multiplexing or polarization-division multiplexing technique was demonstrated to avoid aliasing and improve spatial resolution [12], [13]. The imaging system equipped with Nomarski prism could efficiently retrieve differential phase shifts of a transparent object from two polarized beams and enhance the image contrast [14]. Asymmetric-detection time-stretch optical microscopy could separately reveal enhanced phase-gradient and absorption contrast from two time-multiplexed signals [15].

In the time-stretch imaging technique, a high speed analog-to-digital converter (ADC) is required to sample the detected signal that carries the image information. The image quality is related to the temporal sampling rate. The higher the sampling rate, the larger number of samples can be collected. Hence, more detailed information can be captured from the signal. However, an unintended consequence of the high sampling rate is the huge amount of data. The massive data imposes heavy burden to the following data processing and storage, which stimulates research interests to develop innovative data compression methods. A recent attempt realized optical data compression in the time-stretch imaging system by exploiting the sparsity of the image and nonlinear group delay dispersion, and three times reduction of the data was achieved [16]. A compressive sensing

Manuscript received July 11, 2017; revised September 25, 2017 and October 27, 2017; accepted October 27, 2017. Date of publication October 31, 2017; date of current version November 16, 2017. This work was supported by the National Key Research and Development Program of China (2016YFD0500603), the National Natural Science Foundation of China under Grant 61378060 and Grant 61601292, Yangtze River Delta Joint Project of Shanghai Science and Technology Commission (16395810500), and the Chenguang Project of the Shanghai Municipal Education Commission (14CG45). *(Corresponding author: Xu Wang.)*

B. Dai, S. Yin, Z. Gao, K. Wang, D. Zhang, and S. Zhuang are with the Engineering Research Center of Optical Instrument and System, Ministry of Education, Shanghai Key Laboratory of Modern Optical System, University of Shanghai for Science and Technology, Shanghai 200093, China(e-mail: lioneldai2014@163.com; bensonchaos@163.com; zhensen_gao@163.com; friedrich_suse@foxmail.com; dwzhang@usst.edu.cn; slzhuang@yahoo.com).

X. Wang is with the Institute of Photonics and Quantum Sciences, School of Engineering and Physical Sciences, Heriot-Watt University, Edinburgh EH14 4AS, U.K. (e-mail: x.wang@hw.ac.uk).

Color versions of one or more of the figures in this paper are available online at http://ieeexplore.ieee.org.

Digital Object Identifier 10.1109/JLT.2017.2768382

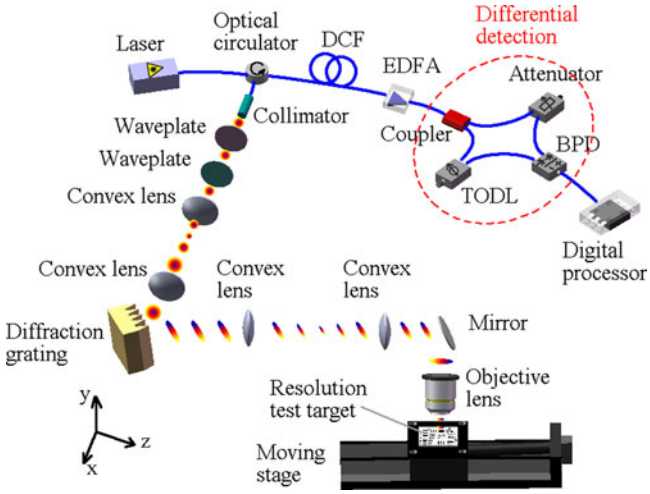

Fig. 1. Schematic of the proposed imaging system. DCF: dispersion compensation fiber. EDFA: erbium-doped fiber amplifier. TODL: tunable optical delay line. BPD: balanced photodetector.

technique was applied to the time-stretch imaging system to simultaneously achieve bandwidth reduction of ADC and sixteen-fold image compression [17]. However, the data compression by using compressive sensing technique was lossy, which degraded the fidelity of the image, and the computation complexity for the data decompression and image reconstruction is high.

In this letter, we propose and experimentally demonstrate a novel high-speed data compression scheme for the time-stretch imaging technique by using differential detection technique [18] and run-length encoding algorithm.

II. Imaging System and Operation Principle

Fig. 1 shows the schematic of the proposed scheme. A broadband laser is used to generate a train of short pulses. The light is output to the free space from a collimator via an optical circulator. Then, the light passes through two waveplates (λ/2 and λ/4 waveplates) for polarization control and two convex lenses for beam expansion. After that, a diffraction grating is employed to spatially disperse the light for wavelength-to-space mapping. The dispersed light is focused to the target by a group of lenses. The intensity of the dispersed light is modulated according to the reflectivity of the target pattern. After capturing the image, the light is reflected back along the same optical path and coupled into a dispersion compensation fiber (DCF) via the optical circulator for wavelength-to-time mapping. After the optical pulses are stretched in the time domain, a 3 dB coupler is used to split the optical pulse into two branches for differential detection. In the one branch, the optical pulses are delayed by *1/R*, where *R* is the scan rate of the imaging system. In the other branch, the intensity of the optical pulses is slightly attenuated to balance the optical power in the both branches. In the image read-out stage, a balanced photodetector (BPD) is used. The BPD consists of two photodiodes with a difference amplifier. Thus, during the optical-to-electrical conversion, the BPD figures out the intensity difference of the optical signals from the two branches. The output electrical signal is then fed into a digitizer for data compression. Run-length encoding algorithm is used to reduce the data volume.

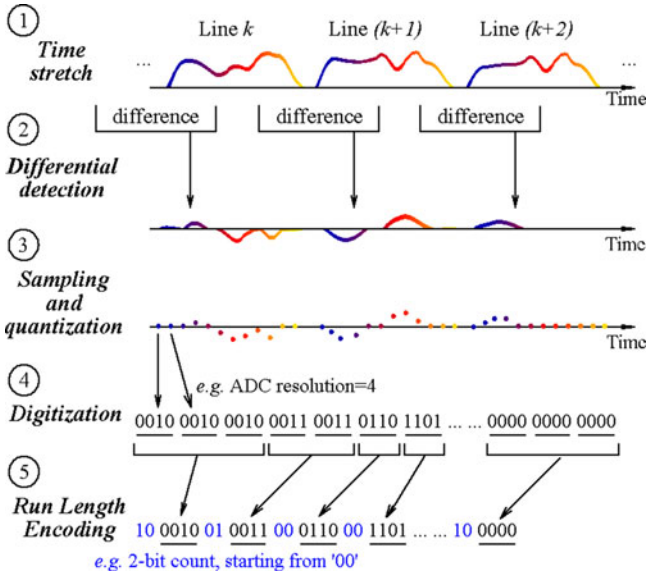

Fig. 2. Operation principle of the data compression scheme.

The operation principle of the data compression scheme is illustrated in Fig. 2. The data compression is achieved by the combination of differential detection and run-length encoding algorithm. After temporally stretching the optical pulses, the image is mapped into the time domain. Differential detection compares the images from the previous scan and the current scan. The same parts of the images are cancelled and the difference of the images is output. If the consecutive scans have high similarity, the output intensity is low. Therefore, the output of differential detection is related to the similarity of the image. In some practical applications, the data from two consecutive scans are almost identical and the difference only occurs in a small portion of the scans. As a result, the output of differential detection is at a very low voltage level and even there is no output.

Before digital signal processing, ADC is required. Each sample is represented by a sequence of binary digits. The sampling rate has the influence over the pixel number for each scan and the ADC resolution, N_{ADC}, determines the number of binary digits for each pixel. In the run-length encoding, a sequence of consecutive identical data is stored as a single data and a count which records the number of the identical data. The size of the count is N_{Count} and the number of the count used for data compression is N_P.

For an image of the pixel number of $N_X \times N_Y$, the original data volume, N_D, is $N_X \times N_Y \times N_{\mathrm{ADC}}$, and the data volume after the data compression, N_C, can be expressed as $N_P \times (N_{\mathrm{Count}} + N_{\mathrm{ADC}})$. The compression ratio is defined as N_D/N_C.

The experiment is based on the setup shown in Fig. 1. A train of optical pulses are generated from a passively mode locked laser with the center wavelength of 1557 nm, –10 dB bandwidth of 8 nm, pulse width of 80 fs (full-width at half maximum) and pulse repetition rate of 155.52 MHz. The repetition rate is down-converted to 77.76 MHz by employing intensity modulation. The beam waist (the radius where intensity falls to $1/\mathrm{e}^2$) from the optical circulator is 1.8 mm and then expanded to 7.2 mm by a pair of convex lenses with focal length of 15 mm and 60 mm.

The diffraction grating has the groove density of 600 lines/mm. After that, a pair of convex lenses with focal length of 30 mm and 15 mm is used to resize the beam waist and couple the light into an objective lens. A USAF-1951 standard resolution test target is placed on the translation stage, which moves perpendicularly to the dispersed light at the speed of 20 cm/s.

In the experiment, the first scan is recorded as a reference line for image reconstruction. After image acquisition, the light is reflected back and input into a span of DCF. The DCF has the length of 12.1 km and the chromatic dispersion is 130 ps/nm • km. Thus, in the wavelength-to-time mapping, the signal is stretched at a rate of 1.573 ns/nm. After signal amplification by using an erbium doped fiber amplifier (EDFA), the optical pulses are divided into two branches for differential detection and conventional detection. In the differential detection, a tunable optical delay line (TODL) is set to 12.86 ns delay in the one branch and an optical attenuator is used in the other branch for power balance. Then, a BPD of 50 GHz bandwidth is employed to figure out the difference between two consecutive scans. As for the conventional detection, a single-pixel photodetector of 50 GHz bandwidth is used to read out the signal directly. Finally, the signal is processed by an oscilloscope with bandwidth of 4 GHz and sampling rate of 20 GS/s.

Fig. 3(a) shows the waveform of the dispersed pulses directly detected by a single-pixel photodetector. The time-stretched pulses are embedded with the spectrum of the laser which has a bell-shaped profile. By eliminating the spectrum profile of the laser from the detected waveform, the image pattern can be figured out. The calculated result is shown in Fig. 3(b). Three rectangular pulses within the time duration of 12.86 ns represent the three reflective horizontal lines on the target. Since the pattern of the reflective lines has no change, every scan captures the same signal and the waveforms are almost same. In the conventional time-stretch imaging system, every sample from the waveforms needs to be recorded to reconstruct the original image, which produces a large amount of data volume and requires large memory storage. Fig. 3(c) depicts the waveforms measured by using differential detection. The waveform is not the image pattern, but the difference between the consecutive scans. Since the consecutive scans are similar, most signals are cancelled, remaining some very low-voltage outputs for several small differences. The positive and negative voltage is related to the increase and decrease of the reflectivity of the target pattern. The cancellation of the consecutive scans makes the received signal at almost the same level and it would be efficient for data compression by using run-length encoding.

III. Experimental Verification

A. Imaging of Resolution Test Target

The bright-field microscopic image of the target used in the experiment is shown in Fig. 4(a). The target is a pattern of the group 4 element 6 of the USAF-1951 standard resolution test target. Each chrome line has the width of 17.5 μm. In the experiment, the objective lens in the imaging system for detecting the standard resolution test target has focal length of 10 mm. The conversion factor between space and wavelength is 6.84 μm/nm

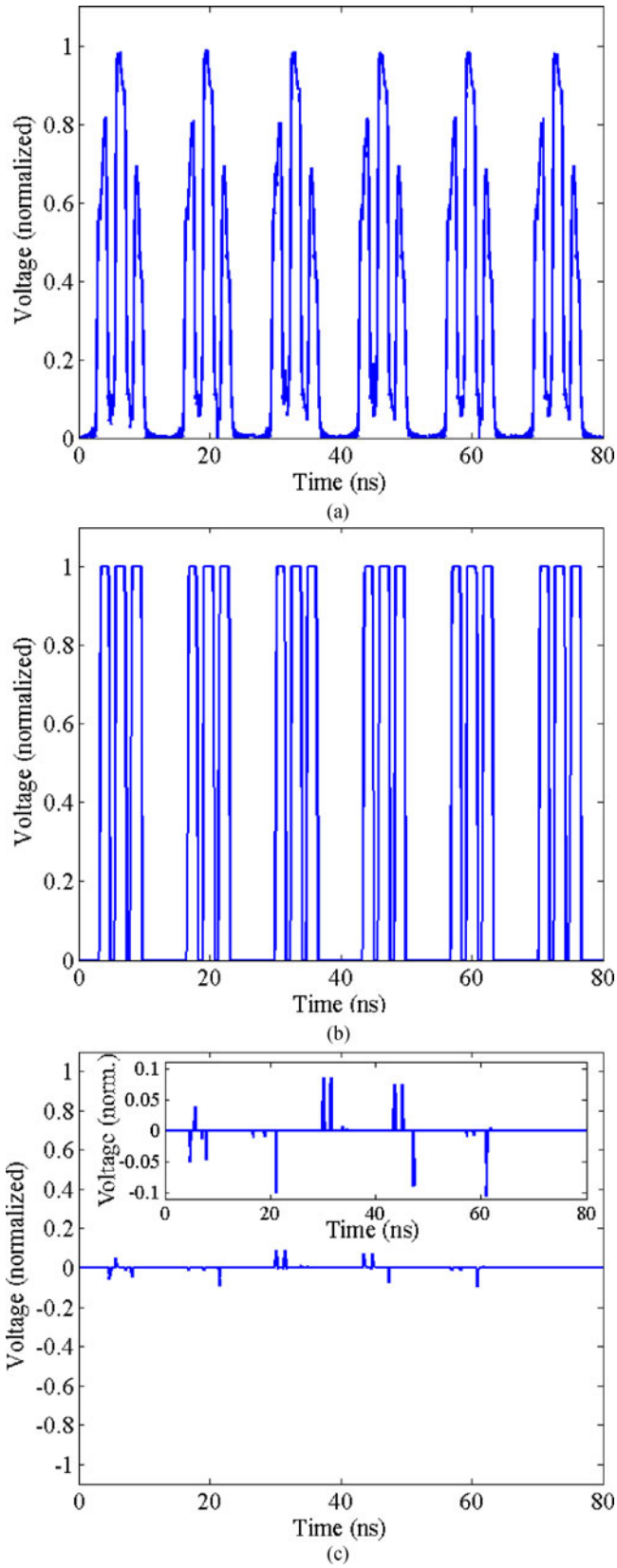

Fig. 3. (a) The measured stretched signals by conventional detection. (b) The signal measured by conventional detection after eliminating the spectrum profile of the laser. (c) The measured stretched signals by differential detection. Inset: The stretched signals detected by differential detection in a magnified vertical scale.

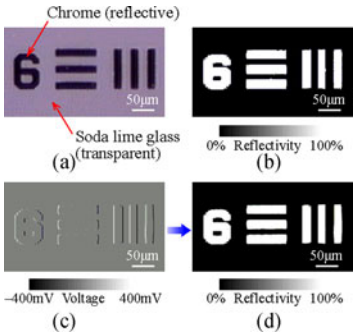

Fig. 4. (a) The bright-field microscopic image of the group 4 element 6 of the USAF-1951 standard resolution test target. (b) The image obtained by the single-pixel detection. (c) and (d) The images obtained by the differential detection and after reconstruction. The numerical aperture (NA) of the objective lens is 0.4.

[19]. Fig. 4(b) shows the image captured by using a single-pixel photodetector. The size of the image is 200 × 250 pixels (scan direction × moving direction). The image is reconstructed from the detected waveforms. The reflectivity of the image directly corresponds to the amplitude of the waveform. The file size of the image is 48.83 KB.

Fig. 4(c) shows the image plotted based on the measured differential data. Most areas of the image including background, number and lines are gray, corresponding to zero-voltage output. Only contours of the number and lines are in white or black. It indicates that most consecutive scans have identical information and the changes occurred at contours of the pattern are found. Since most consecutive data are identical, it is very efficient to use run-length encoding algorithm to compress the data. The count size, N_{Count}, used in the demonstration is 8 bits. The file size after the data compression becomes 4.32 KB. Comparing to the data volume in the conventional time-stretching imaging system, the compression ratio is 11.3.

In the image reconstruction, the encoded data is firstly decompressed by using run-length decoding algorithm to recover the differential data. Then, the reference line is used as the first line of the image and the remaining part of the image is reconstructed line-by-line by adding the differential data of each line to the latest reconstructed line of the image starting from the reference line. The reconstructed image has high image quality, as shown in Fig. 4(d). Since the thermal noise and shot noise in the BPD are very low comparing to the signal, the detected signal is not corrupted by the noise. Besides, there is no data loss in the run-length encoding. Therefore, the high fidelity of the image can be guaranteed. According to Shannon's information theory, the entropy of the images in Fig. 4(c) and (d) is 1.07 and 1.41, respectively. It indicates that the image in Fig. 4(c) has more redundancy than that in Fig. 4(d) does and the differential detection can improve the compressibility.

B. Imaging of Red Blood Cells

A demonstration of gray-scale image detection is further conducted. The setup of the imaging system is modified as shown in Fig. 5. After light diffraction and beam size adjustment, the light is coupled into a pair of objective lenses, which are used to capture the microscopic image in the channel of the microfluidic chip. The objective lenses for cell detection have numerical aperture of 0.65 and focal length of 4 mm. The space-to-wavelength conversion factor is 2.74 μm/nm. A mirror placed after the second objective lens is to reflect the light back. Human red blood cells (RBCs) are injected into a microfluidic chip, whose channel has width of 50 μm and height of 30 μm. The flow rate is 2 m/s. In the wavelength-to-time mapping stage, the optical power before and after the amplification is 27 μW and 632 μW, respectively.

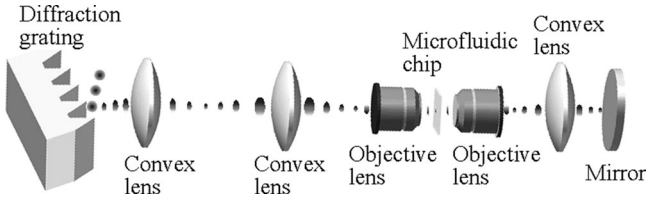

Fig. 5. The setup of the imaging system for cell detection. The NA of the objective lenses is 0.65.

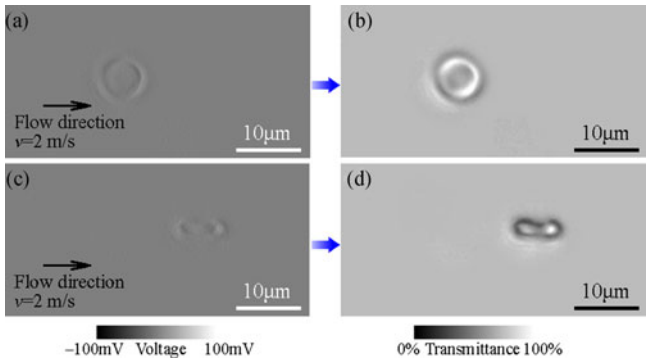

Fig. 6. (a) and (c) The images obtained by the differential detection. (b) and (d) The images after reconstruction.

The images obtained by the differential detection are shown in Fig. 6(a) and (c). The image is mainly in gray, indicating that the most similar parts are canceled and only the difference between adjacent scans remains. The image size is 200 × 400 pixels (scan direction × flow direction). The count size used in the data compression is 8 bits. The compression ratios of 3.8 and 4.4 are achieved for the two cases, respectively. Fig. 6(b) and (d) show the reconstructed images. The images of RBCs present high contrast and resolution. The biconcave shapes of the RBCs can be clearly observed. The images after differential detection, Fig. 6(a) and (c), have entropy of 1.18 and 0.86 and the reconstructed images, Fig. 6(b) and (d), have entropy of 1.72 and 1.47.

IV. Efficiency of Data Compression

A. System Setup

In the data compression, the image is stored as groups of counts and single data. Therefore, the count size and the size of the single data, which is determined by the ADC resolution, N_{ADC}, have the influence over the data volume as well as the compression ratio. Fig. 7 illustrates the efficiency of the data compression for the imaging of the resolution test target as demonstrated in Section III. The compression ratio is analyzed when different count size and ADC resolution are used to process the data with conventional detection and differential

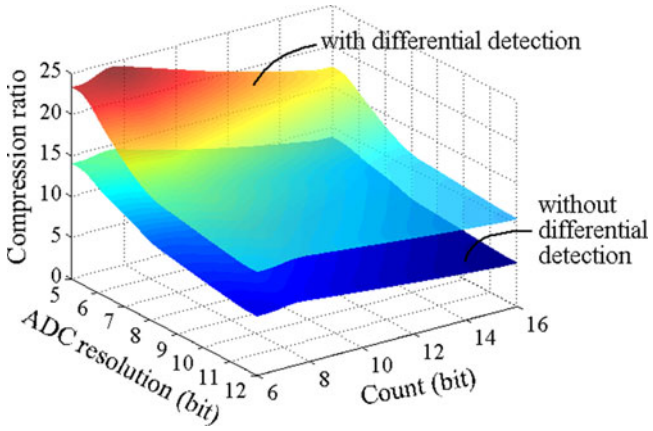

Fig. 7. Compression ratio for different ADC resolution and count size with and without differential detection.

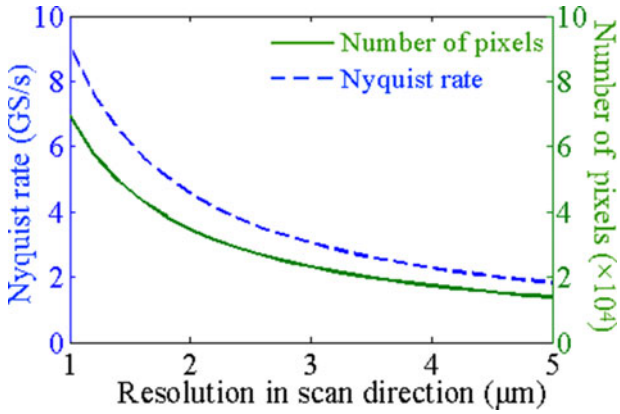

Fig. 8. The influence of the resolution over the Nyquist rate and the number of pixels.

detection. The compression ratio for the case using the conventional single-pixel detection is calculated with the data after eliminating the spectrum profile of the laser. It is obvious that the imaging system with differential detection can achieve higher compression ratio by almost two fold. The differential detection is capable of eliminating identical information of consecutive scans and distinguishing discrepancy. Once the consecutive scans are similar or identical, the output voltage of differential detection is almost at the same level, especially when ADC resolution is low. Then, it becomes more efficient for run-length encoding algorithm to merge the signals at the same-voltage level to a single data.

Furthermore, a proper count size is necessary to count the number of identical consecutive data. Although the count of a small size has fewer digits, it is not suitable for counting a long sequence of identical consecutive data because the data volume might be increased when overflow of the count happens and then more counts are needed. Besides, high ADC resolution promises high image quality, but it not only requires more digits to record a signal but also makes it inefficient for run-length encoding algorithm to compress the data since the possibility of identical consecutive data is reduced.

Spatial resolution is a key factor in the imaging system, which is closely related to the image quality. The resolution along the scan direction is mainly determined by the focal length of the objective lens, input beam size, diffraction of the grating and chromatic dispersion for time stretch, while the resolution along the flow direction is affected by the focal length of the objective lens and input beam size [19]. In the time-stretch imaging system, the spatial resolution is a criteria for signal sampling. Theoretically, signals can be sampled at Nyquist rate, i.e., $f_{\text{Nyquist}} = 2f/[d\cos(\theta_g)D\delta x]$, where f is the focal length of the objective lens, d is the grating period, θg is the diffracted angle under Littrow's condition, D is the group velocity dispersion and δx is the spatial resolution along the scan direction. In the calculation, the resolution is adjusted by changing the input beam size in the two directions because the change of the beam size does not affect other system performance such as field-of-view and temporal resolution. Gaussian-shaped beam is used. The space-to-wavelength and wavelength-to-time conversion factors are 6.84 μm/nm and 1.5 ns/nm, respectively. Fig. 8 shows the influence of the resolution over the required Nyquist rate and the number of pixels. With the degradation of the resolution, the required sampling rate becomes low because the temporal resolution of the system degrades as well resulting in a narrow signal bandwidth. In addition, the image size can be significantly reduced when the signal is sampled at Nyquist rate especially when the spatial resolution is low.

Fig. 9 shows the influence of the resolution along the scan and moving directions over the compression ratio and the image quality. The target image has both binary and gray-scale patterns, as shown in Fig. 9(a). The size of the image is about 130 μm $\times$ 200 μm (scan direction $\times$ moving direction). The ADC is operated at both 20 GS/s sampling rate and Nyquist rate. Fig. 9(b) and (c) show the compression ratio and peak signal-to-noise ratio (PSNR) with the change of the resolution along the scan direction and the moving direction. In the calculation of the PSNR, the target image is resized for the comparison with the reconstructed images obtained at different sampling rate. The reconstructed images are illustrated in Fig. 9(d)–(g). When the resolution is low, the reconstructed images become blurry and the compression ratio decreases. With the degradation of the resolution, the PSNR keeps decreasing and the compression ratio converges to a certain value because the signal obtained by the differential detection tends to a similar value and the corresponding image turns to blurred gray color, as shown in the inset of Fig. 9(b). In contrast to the signal sampled at Nyquist rate, the signal obtained at 20 GS/s has better image quality and can be compressed more efficiently. Hence, it is necessary to balance the tradeoff between the image quality and the data size by setting a proper sampling rate. Besides that, high resolution is preferred to ensure high image quality and compression ratio.

B. Intensity Noise and Timing Jitter

In the imaging system, if the laser source or reference clock is unstable, intensity noise and timing jitter due to the spectrum fluctuation and repetition rate drift of the laser source or the clock affect the system performance. In the calculation, random intensity noise and timing jitter are induced into the imaging system. The resolution in the both scan and moving directions is set to 1 μm. Fig. 10(a)–(d) show the images

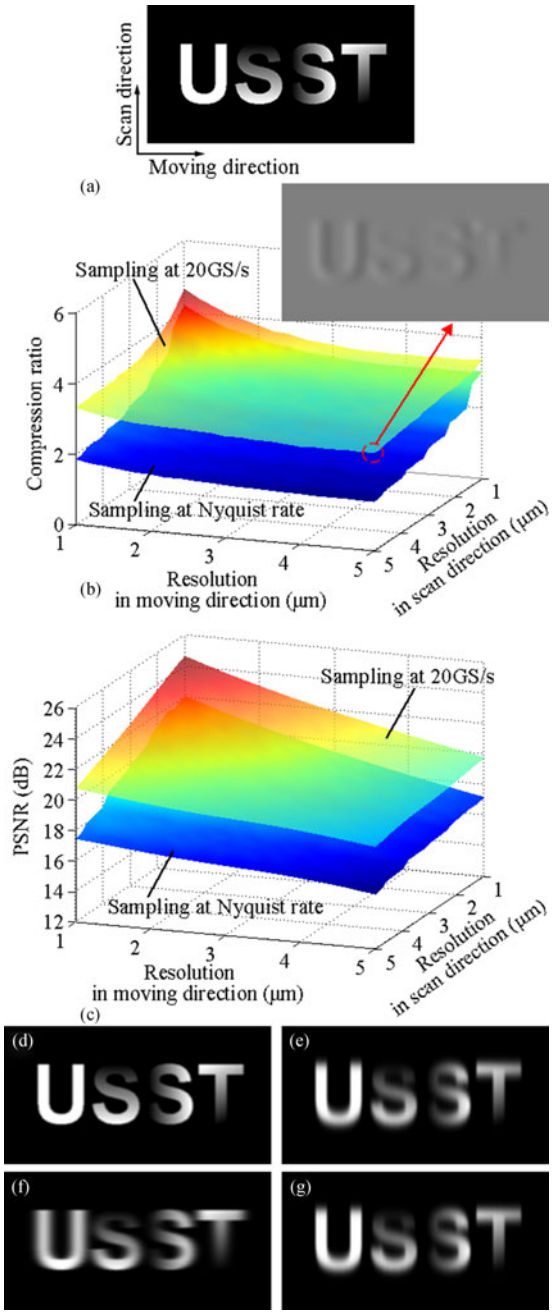

Fig. 9. (a) The target image used for calculation. (b) Compression ratio and (c) peak signal-to-noise ratio for different resolution along scan direction and moving direction. Inset: the image obtained by differential detection when the resolution along both scan and moving directions is 5 μm. The reconstructed images when the resolution is (d) 1 μm in both scan and moving directions, (e) 5 μm in scan direction and 1 μm in moving direction, (f) 1 μm in scan direction and 5 μm in moving direction, and (g) 5 μm in both scan and moving directions.

obtained by the differential detection and the reconstructed images when the deviation of the intensity fluctuation of the spectrum and the timing jitter is 5%, respectively. Due to the existence of the intensity noise, the detected signal fluctuates randomly and the reconstructed image is corrupted by salt-and-pepper noise. The image reconstructed from the signals that experience the timing jitter is distorted along the scan direction owing to the temporal misalignment.

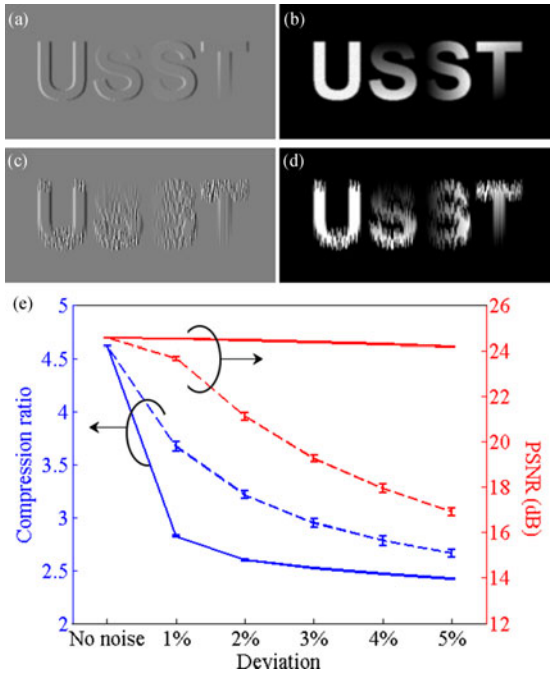

Fig. 10. (a) The image obtained by differential detection and (b) the reconstructed image with the existence of 5% intensity noise. (c) The image obtained by differential detection and (d) the reconstructed image with the existence of 5% timing jitter. (e) The influence of intensity noise and timing jitter over the compression ratio and PSNR. Solid lines: intensity noise. Dashed lines: timing jitter.

Fig. 10(e) shows the influence of the noise over the compression ratio and the image quality. The error bars are standard deviation for the identical deviation of the random noise in the 50 different runs. The compression ratio drops dramatically with the increase of the intensity noise because the intensity fluctuation results in that adjacent pixels have more intensity levels which makes run-length encoding inefficient. In the case of timing jitter, the signals from the consecutive line scans cannot be cancelled in the differential detection and the compressibility of the signal becomes low. In addition, the image quality degrades by about 7 dB when the timing jitter deteriorates by 5% because the reconstructed image is distorted severely, while the intensity noise has slight influence over the image quality. The imaging system equipped with a laser source of highly stable optical spectrum and repetition rate can not only guarantee image quality but also achieve high compression ratio.

V. Discussion

The proposed data compression method is applicable in the existing time-stretch imaging system by simply replacing single-pixel photodetection with differential detection. The data compression method has following features. The differential detection figures out the similarity between the two consecutive signals in real time, while the low-computation-complexity run-length encoding merges the identical consecutive data into a single data one by one. It is not necessary to completely store all data and then compress the data by statistically eliminating redundancy, which is suitable for fast online data compression. It is worth noting that the proposed method is image pattern re-

lated just like the method in [16], in which warped group delay dispersion for time stretch depended on the sparsity of the image. In the proposed scheme, data compression ratio is related to the image pattern and the method is suitable to process the image with identical consecutive scans or identical changes of the scans. In addition, comparing to the data compression method in [17], the proposed method detects every sample of the signal in differential format and no image information is lost during the data compression. Thus, the fidelity can be guaranteed.

VI. Conclusion

In conclusion, the time-stretch imaging system with differential detection and run-length encoding is proposed for data compression. The differential detection eliminates identical signals of consecutive scans and outputs the discrepancy between the scans. After differential detection, the possibility of identical data in the data stream is increased, which benefits to data compression by using run-length encoding. The 77.76 MHz line-scan imaging system is experimentally demonstrated. Comparing to the data volume obtained by the conventional system, the compression ratio of 11.3 is achieved. Since run-length encoding is lossless, the fidelity of the reconstructed image is guaranteed. The proposed scheme can efficiently reduce the data volume and has low computation complexity. It is a promising fast online data compression method for time-stretch imaging system.

Acknowledgment

The authors would like to thank Prof. Guodong Sui and Dr. Lulu Zheng for processing red blood cells.

References

[1] P. Hockett, C. Z. Bisgaard, O. J. Clarkin, and A. Stolow, "Time-resolved imaging of purely valence-electron dynamics during a chemical reaction," *Nature Phys.*, vol. 7, no. 8, pp. 612–615, Apr. 2011.

[2] R. Kodama *et al.*, "Fast heating of ultrahigh-density plasma as a step towards laser fusion ignition," *Nature*, vol. 412, pp. 798–802, Aug. 2001.

[3] K. Goda *et al.*, "High-throughput single-microparticle imaging flow analyzer," *PNAS*, vol. 109, no. 29, pp. 11630–11635, Jun. 2012.

[4] M. E. Desouki, M. J. Deen, Q. Fang, L. Liu, F. Tse, and D. Armstrong, "CMOS image sensors for high speed applications," *Sensors*, vol. 9, no. 1, pp. 430–444, Jan. 2009.

[5] U. Frühling *et al.*, "Single-shot terahertz-field-driven X-ray streak camera," *Nature Photon*, vol. 3, no. 9, pp. 523–528, Aug. 2009.

[6] C. Porneala and D. A. Willis, "Observation of nanosecond laser-induced phase explosion in aluminum," *Appl. Phys. Lett.*, vol. 89, Nov. 2006, Art. no. 211121.

[7] K. Goda, K. K. Tsia, and B. Jalali, "Serial time-encoded amplified imaging for real-time observation of fast dynamic phenomena," *Nature*, vol. 458, pp. 1145–1149, Apr. 2009.

[8] K. Goda *et al.*, "Hybrid dispersion laser scanner," *Sci. Rep.*, vol. 2, Jun. 2012, Art. no. 445.

[9] B. Dai, D. Wang, Q. Wang, R. J. Hong, D. W. Zhang, and X. Wang, "Ultrafast three-dimensional imaging system based on phase-shifting method and hybrid dispersion laser scanning," *Photon. J.*, vol. 7, no. 3, pp. 1–9, Apr. 2015.

[10] H. Chen *et al.*, "Multiwavelength time-stretch imaging system," *Opt. Lett.*, vol. 39, no. 7, pp. 2202–2205, Mar. 2014.

[11] G. Wang, C. Wang, Z. Yan, and L. Zhang, "Highly efficient spectrally encoded imaging using a 45° tilted fiber grating," *Opt. Lett.*, vol. 41, no. 11, pp. 2398–2401, May 2016.

[12] B. Dai *et al.*, "Ultrafast imaging with anti-aliasing based on optical time-division multiplexing," *Opt. Lett.*, vol. 41, no. 5, pp. 882–885, Feb. 2016.

[13] F. J. Xing, H. W. Chen, S. Z. Xie, and J. P. Yao, "Ultrafast surface imaging with an increased spatial resolution based on Polarization-Division multiplexing," *J. Lightw. Technol.*, vol. 33, no. 2, pp. 396–402, Jan. 2015.

[14] A. M. Fard, A. Mahjoubfar, K. Goda, D. R. Gossett, D. D. Carlo, and B. Jalali, "Nomarski serial time-encoded amplified microscopy for high-speed contrast-enhanced imaging of transparent media," *Biomed. Opt. Express*, vol. 2, no. 12, pp. 3387–3392, Nov. 2011.

[15] T. T. W. Wong *et al.*, "Asymmetric-detection time-stretch optical microscopy (ATOM) for ultrafast high-contrast cellular imaging in flow," *Sci. Rep.*, vol. 4, Jan. 2014, Art. no. 3656.

[16] C. L. Chen, A. Mahjoubfar, and B. Jalali, "Optical data compression in time stretch imaging," *Plos One*, vol. 10, no. 4, Apr. 2015, Art. no. e0125106.

[17] Q. Guo, H. Chen, Z. Weng, M. Chen, S. Yang, and S. Xie, "Compressive sensing based high-speed time-stretch optical microscopy for two-dimensional image acquisition," *Biomed. Opt. Express*, vol. 23, no. 23, pp. 29639–29646, Nov. 2015.

[18] B. Dai, Z. Gao, X. Wang, N. Kataoka, and N. Wada, "Demonstration of differential detection on attacking code-shift-keying OCDMA system," *Electron. Lett.*, vol. 46, no. 25, pp. 1680–1682, Dec. 2010.

[19] K. K. Tsia, K. Goda, D. Capewell, and B. Jalali, "Performance of serial time-encoded amplified microscope," *Opt. Express*, vol. 18, no. 10, pp. 10016–10028, Apr. 2010.

Bo Dai received the B.Eng. (First-class Honors) degree from the College of Science and Engineering, City University of Hong Kong, Hong Kong, in 2009, and the Ph.D. degree from the Institute of Photonics and Quantum Sciences, Heriot-Watt University, Edinburgh, U.K., in 2013. From 2011 to 2012, he was with the National Institute of Information and Communications Technology, Japan, as an Internship Research Fellow. He is currently an Associate Professor with the University of Shanghai for Science and Technology, Shanghai, China.

Songchao Yin received the B.S. degree in electronic and information engineering from Hunan Institute of Science and Technology, Yueyang, China, in 2015. He is currently working toward the master's degree in signal and information processing with the University of Shanghai for Science and Technology, Shanghai, China. His research interests include ultrafast imaging systems.

Zhensen Gao received the B.S. and M.S. degrees in physics from Harbin Institute of Technology, Harbin, China, in 2006 and 2008, respectively, and the Ph.D. degree in electronics engineering from Heriot-Watt University, Edinburgh, U.K., in 2011. He is currently a Researcher with the University of Shanghai for Science and Technology, Shanghai, China.

Kaimin Wang received the Ph.D. degree from Beijing University of Posts and Telecommunications, Beijing, China, in 2016. He is currently a Lecturer with the University of Shanghai for Science and Technology, Shanghai, China.

Dawei Zhang received the Ph.D. degree from Shanghai Institute of Optics and Fine Mechanics, Chinese Academy of Sciences, Shanghai, China, in 2005. He is a Professor and Director of the Optical Instrument and Systems Engineering Center, University of Shanghai for Science and Technology, Shanghai. He has been a Senior Visiting Scholar with Nanyang Technological University, Singapore, since 2012.

Songlin Zhuang received the Ph.D. degree from Pennsylvania State University, State College, PA, USA, in 1982. He is an academician with the China Academy of Engineering, a Professor with the University of Shanghai for Science and Technology, Shanghai, China, the Dean of the Institute of Optoelectronic Information and Computer Engineering, University of Shanghai for Science and Technology, and the Director of Shanghai Institute of Optical Instruments. He is also the Chairman of the China Instrument and Control Society and the Director of the Chinese Optical Society.

Xu Wang received the Ph.D. degree in electronic engineering from the Chinese University of Hong Kong (CUHK), Hong Kong. He has worked with the National Key Laboratory of Fiber Optic Broad-band Transmission and Communication Networks, University of Electronic Science and Technology of China, China; the Department of Electronic Engineering, CUHK; the Department of Electronic and Information Systems, Osaka University, Osaka, Japan; and the Photonic Network Group, National Institute of Communication and Information Technology, Tokyo, Japan. He is currently an Associate Professor with the Institute of Photonics and Quantum Sciences, Heriot-Watt University, Edinburgh, U.K.